

Regulation of myelin structure and conduction velocity by perinodal astrocytes

Dipankar J. Dutta^{a,b}, Dong Ho Woo^a, Philip R. Lee^a, Sinisa Pajevic^c, Olena Bukalo^a, William C. Huffman^a, Hiroaki Wake^a, Peter J. Bassar^d, Shahriar SheikhBahaei^e, Vanja Lazarevic^f, Jeffrey C. Smith^e, and R. Douglas Fields^{a,1}

^aSection on Nervous System Development and Plasticity, The Eunice Kennedy Shriver National Institute of Child Health and Human Development, National Institutes of Health, Bethesda, MD 20892; ^bThe Henry M. Jackson Foundation for the Advancement of Military Medicine, Inc., Bethesda, MD 20817; ^cMathematical and Statistical Computing Laboratory, Office of Intramural Research, Center for Information Technology, National Institutes of Health, Bethesda, MD 20892; ^dSection on Quantitative Imaging and Tissue Sciences, The Eunice Kennedy Shriver National Institute of Child Health and Human Development, National Institutes of Health, Bethesda, MD 20892; ^eCellular and Systems Neurobiology Section, National Institute of Neurological Disorders and Stroke, National Institutes of Health, Bethesda, MD 20892; and ^fExperimental Immunology Branch, National Cancer Institute, National Institutes of Health, Bethesda, MD 20892

Edited by Terrence J. Sejnowski, Salk Institute for Biological Studies, La Jolla, CA, and approved September 25, 2018 (received for review June 26, 2018)

The speed of impulse transmission is critical for optimal neural circuit function, but it is unclear how the appropriate conduction velocity is established in individual axons. The velocity of impulse transmission is influenced by the thickness of the myelin sheath and the morphology of electrogenic nodes of Ranvier along axons. Here we show that myelin thickness and nodal gap length are reversibly altered by astrocytes, glial cells that contact nodes of Ranvier. Thrombin-dependent proteolysis of a cell adhesion molecule that attaches myelin to the axon (neurofascin 155) is inhibited by vesicular release of thrombin protease inhibitors from perinodal astrocytes. Transgenic mice expressing a dominant-negative fragment of VAMP2 in astrocytes, to reduce exocytosis by 50%, exhibited detachment of adjacent paranodal loops of myelin from the axon, increased nodal gap length, and thinning of the myelin sheath in the optic nerve. These morphological changes alter the passive cable properties of axons to reduce conduction velocity and spike-time arrival in the CNS in parallel with a decrease in visual acuity. All effects were reversed by the thrombin inhibitor Fondaparinux. Similar results were obtained by viral transfection of tetanus toxin into astrocytes of rat corpus callosum. Previously, it was unknown how the myelin sheath could be thinned and the functions of perinodal astrocytes were not well understood. These findings describe a form of nervous system plasticity in which myelin structure and conduction velocity are adjusted by astrocytes. The thrombin-dependent cleavage of neurofascin 155 may also have relevance to myelin disruption and repair.

myelin plasticity | node of Ranvier | thrombin | neurofascin 155 | spike-time-dependent plasticity

Conduction velocity (CV) is increased in axons with thicker myelin sheaths, and the length of the nodal gap and distribution of Na⁺ channels in the node of Ranvier have a strong influence on the action potential firing threshold, frequency of firing, and CV (1). More than 95% of nodes of Ranvier in the CNS are contacted by astrocytes (2), but the function of perinodal astrocytes remains a long-standing question (3). The possibility that astrocytes could participate in maintaining or remodeling myelin structure was explored using transgenic mice and by viral gene transfection in rats.

The myelin sheath attaches to the axon by forming a spiral junction in the paranodal region flanking the node of Ranvier (Fig. 1A), which has the appearance of a series of loops when sectioned longitudinally for electron microscopy (EM). Paranodal loops promote action potential propagation by concentrating Na⁺ channels in the node, preventing juxtaparanodal K⁺ channels from diffusing into the node (4), and narrowing the nodal gap length to increase membrane resistivity and reduce capacitance (5). Paranodal loops are attached to the axon via septate-like junctions (Fig. 1B) composed of a complex of three intercellular proteins, with neurofascin155 (NF155) on the paranodal loop interacting with the Contactin1-associated protein1 (Caspr1)/Contactin1 complex on the axon (Fig. 1C) (6). We tested the hypothesis that this point of axo-

glial contact can be modified by vesicular release of substances from astrocytes and that this could enable astrocytes to influence nodal structure, myelin sheath thickness, and impulse conduction speed.

Results

Astrocyte Exocytosis Inhibits Thrombin-Mediated Cleavage of NF155.

Our bioinformatic analysis revealed a potential proteolytic cleavage site in the extracellular domain of mouse NF155 after arginine, amino acids 924–926 (glycine–arginine–glycine), that is specific for the enzyme thrombin (*SI Appendix, Fig. S1A*) (7). Molecular modeling showed that the cleavage site is on the surface of the protein (Fig. 1C and *Movie S1*), accessible to thrombin (*SI Appendix, Fig. S1B*), and thrombin treatment of subcortical white matter in vitro was found to cleave NF155 at this site (*SI Appendix, Fig. S1C*). Cleavage here would sever the Ig 5–6 domains that interact with Contactin1 (Fig. 1C), thus breaking the attachment of paranodal loops to the axon (8).

Under normal conditions thrombin is secreted by neurons and enters the CNS from the vascular system (9). In the CNS, astrocytes are the primary source of the thrombin inhibitor protease nexin1 (PN1) (also called glial-derived nexin-1 and SERPINE2) (10), suggesting that perinodal astrocytes could modulate myelin

Significance

Proper communication between brain regions, via white matter tracts, allows us to carry out complex cognitive and motor tasks. Impulses traveling must arrive at relay points almost simultaneously for such communication to be effective. Myelin enables saltatory conduction of impulses and hence is a candidate for modulation of impulse conduction velocity. But myelin structure, once formed, has been considered static. In this study, we show that mature myelin structure is dynamic. The mature myelin sheath thickness and nodal gap length can be reversibly modulated to optimize the speed of axonal impulses. This modulation of myelin is regulated by exocytosis of thrombin protease inhibitors from astrocytes at the node of Ranvier.

Author contributions: R.D.F. designed research; D.J.D., D.H.W., P.R.L., S.P., O.B., W.C.H., P.J.B., S.S., V.L., and R.D.F. performed research; J.C.S. contributed new reagents/analytic tools; D.J.D., D.H.W., P.R.L., S.P., O.B., W.C.H., H.W., P.J.B., S.S., V.L., and R.D.F. analyzed data; and D.J.D. and R.D.F. wrote the paper.

Conflict of interest statement: The United States Government applied for an international patent (US Patent PCT/US2016/027776) titled, "Methods of treating or preventing demyelination using thrombin inhibitors and methods of detecting demyelination using Neurofascin 155," on April 15, 2016, as the sole beneficiary. R.D.F., D.J.D., and D.H.W. are listed as inventors in the patent application.

This article is a PNAS Direct Submission.

This open access article is distributed under [Creative Commons Attribution-NonCommercial-NoDerivatives License 4.0 \(CC BY-NC-ND\)](https://creativecommons.org/licenses/by-nc-nd/4.0/).

¹To whom correspondence should be addressed. Email: fieldsd@mail.nih.gov.

This article contains supporting information online at www.pnas.org/lookup/suppl/doi:10.1073/pnas.1811013115/-DCSupplemental.

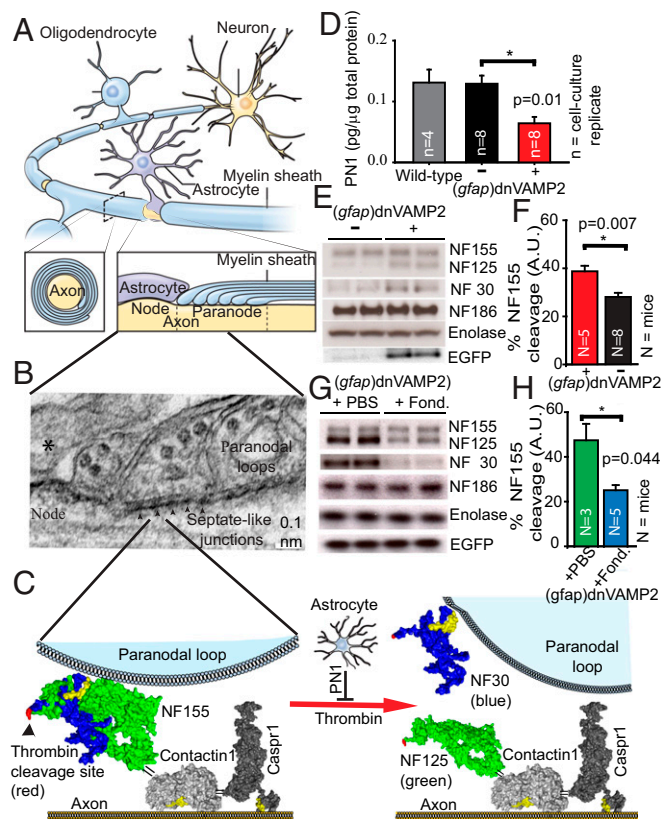


Fig. 1. Secretion of PN1 from astrocytes inhibits thrombin-mediated cleavage of NF155 to regulate attachment of myelin to the axon. (A and B) The myelin sheath is attached to the axon by NF155 in septate junctions (B arrowheads). B is a TEM of adult optic nerve. Astrocytes (*) contact the node. (C) Thrombin cleavage of NF155, inhibited by PN1 and secreted from astrocytes, would sever NF155 attachment of paranodal loops to the axon. Thrombin proteolytic site AA924 (red), short fragment (NF30) (blue), and long fragment (NF125) (green). (D) Reducing exocytosis from astrocytes in culture, by expressing a dominant-negative vesicle-associated membrane protein 2 [(*gfap*)dnVAMP2], reduces Mastoparan-induced PN1 secretion (ANOVA, $F_{2, 19} = 8.15$, $P = 0.003$). (E–H) Increased cleavage of NF155 in subcortical white matter of mice expressing (*gfap*)dnVAMP2 (t test, $t_{11} = 3.315$, E and F) is reversed by the thrombin inhibitor Fondaparinux (t test, $t_4 = 2.9$, G and H). Neurofascin 186, lacking a thrombin cleavage site, and neuron-specific enolase, are controls. EGFP is a reporter of dnVAMP2 expression. Predicted molecular structures of paranodal septate junction proteins in C were determined by I-TASSER (Materials and Methods; Movie S1; SI Appendix, Figs. S1 and S2). A single asterisk (*) indicates a significant difference.

structure by regulating attachment of myelin to the axon. In support of this, 2.20 ± 0.072 pg of PN1/μg tissue was released from excised mouse optic nerve after a 20-min treatment with mastoparan, an activator of G_i/G_o receptors, known to stimulate exocytosis of PN1 from astrocytes (11). In purified cell cultures of astrocytes, PN1 secretion induced by mastoparan was reduced 50% by suppressing VAMP2-dependent exocytosis by using a transgenic mouse expressing a doxycycline (Dox)-regulated dominant-negative cytosolic VAMP2 fragment (dnVAMP2) under control of the astrocyte-specific promoter *GFAP* to drive cell-specific expression (Fig. 1D) (12). (SI Appendix, SI Materials and Methods and Fig. S2 A–K) Expression of the gene, referred to here as (*gfap*)dnVAMP2, is prevented by Dox treatment. In vivo, dnVAMP2 was expressed only in astrocytes and only in the absence of Dox treatment (SI Appendix, Fig. S2 D–I). There were no effects of the transgene on structure and function of retina (SI Appendix, Fig. S3 A–P and Table S1), alteration in axon diameter or number of myelinated axons in optic nerve (SI Appendix, Fig. S3 Q and R), or immunological response (SI Appendix, Fig. S4).

By hypothesis, the 50% reduction in exocytosis of PN1 and other serine protease inhibitors from astrocytes should increase NF155 cleavage at AA924 in white matter of mice expressing (*gfap*)dnVAMP2, and this was confirmed by immunoblot and amino acid sequencing by mass spectrometry (Fig. 1 E and F). No change was found in the other neurofascin family member at the node, neurofascin 186 (NF186), which lacks a thrombin cleavage site. Many substances can be released by exocytosis from astrocytes, but cleavage of NF155 in animals expressing (*gfap*)dnVAMP2 was prevented by daily s.c. injections of the highly specific thrombin inhibitor Fondaparinux, indicating that thrombin proteolysis is responsible for the increased cleavage of NF155 (Fig. 1 G and H). Fondaparinux treatment in the absence of (*gfap*)dnVAMP2 gene expression had no significant effect (SI Appendix, Fig. S5).

Astrocyte Exocytosis Regulates Detachment of Paranodal Loops of Myelin at the Node of Ranvier. Cleavage of NF155 by thrombin should disrupt the axoglial junction holding paranodal loops to the axon, causing them to detach. The optic nerve was chosen for analysis because of its uniform population of myelinated axons from retinal ganglion cells, devoid of dendrites, synapses, or other neurons. High-resolution transmission EM, serial block-face scanning EM (SBSEM), and 3D reconstruction from SBSEM showed many cases in which the outermost paranodal loops of myelin were detached from the axon adjacent to perinodal astrocytes when exocytosis from astrocytes was reduced (Fig. 2 A–G). Paranodal loops more distal to the perinodal astrocyte had normal morphology and prominent septate junctions with the axon (Fig. 2 A–C). Detached paranodal loops were also evident in cross-sectional transmission electron microscopy (TEM) (Fig. 2G) as cytoplasm filled wraps of uncompacted myelin, withdrawn from the node overlying the compacted myelin. This detachment and withdrawal of the outer myelin wraps is clearly evident in high-resolution 3D reconstructions generated from SBSEM (Fig. 2 D–F).

Detachment of paranodal loops was observed less frequently in the wild-type (WT) condition (Fig. 2H) and after restoring normal astrocytic secretion by terminating expression of the transgene by Dox treatment (Fig. 2I). Quantitative TEM analysis of 617 nodes of Ranvier indicated that 38.3% of nodes had paranodal loops detached in mice with astrocytes expressing (*gfap*)dnVAMP2, significantly more than the 20.0% detached when (*gfap*)dnVAMP2 expression was prevented by Dox treatment. The latter condition was not significantly different from WT mice (22.8%) (Fig. 2J). The increased detachment of paranodal loops was reduced to normal by restoring normal levels of exocytosis from astrocytes by resupplying Dox to the diet for 30 d or by daily injections of the thrombin inhibitor Fondaparinux (10 mg/kg) for 3 wk (Fig. 2J). Together, these results show that detachment of paranodal loops is a normal process ongoing in WT mice, which is increased by reducing exocytosis from astrocytes, thereby increasing thrombin-dependent proteolysis of NF155.

Astrocyte Exocytosis Regulates Nodal Gap Length. Detachment of the outermost paranodal loops should increase the nodal gap length, and this was confirmed quantitatively by confocal microscopy following immunohistochemical staining of Na^+ channels marking the nodal gap and Caspr1 marking the paranodal regions (Fig. 3A). Nodal gap length increased significantly in mice with astrocytes expressing (*gfap*)dnVAMP2, but there was no difference between animals on Dox compared with WT (Fig. 3B). Similar results were found when exocytosis from astrocytes was reduced by removing Dox in adult mice, indicating that remodeling of myelin by vesicle release from astrocytes can occur after myelin is fully formed (Fig. 3A and B). Importantly, the increase in nodal gap length in these mice was prevented by daily s.c. injections of the thrombin inhibitor Fondaparinux (10 mg/kg) (Fig. 3A and B). Immunoblot analysis confirmed that NF155 cleavage was prevented in the same animals expressing (*gfap*)

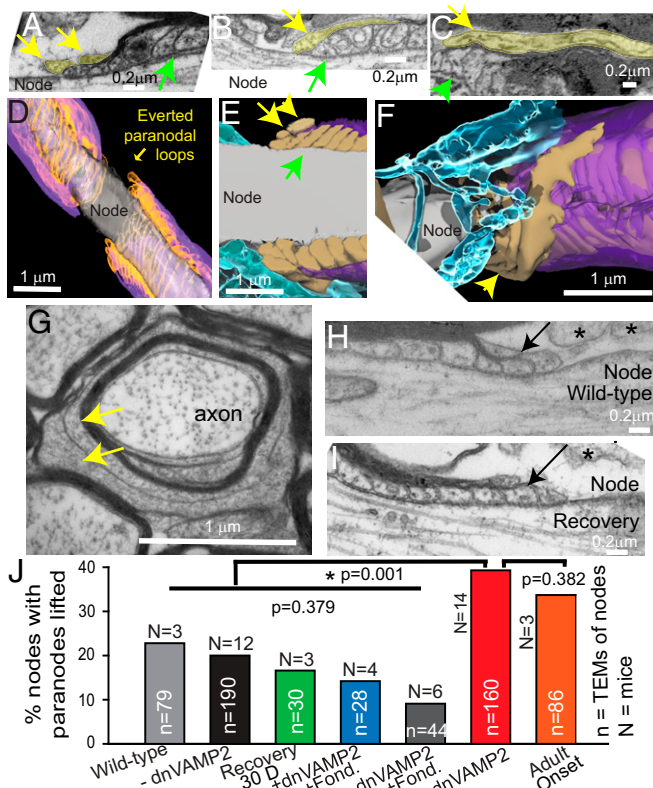


Fig. 2. Detachment of outermost paranodal loops of myelin is regulated by vesicular release of PN1 from astrocytes. (A–C) Detachment of paranodal loop (A), expanded cytoplasm (B), and displacement of the node (C) are shown by EM in mice with exocytosis from astrocytes reduced by (*gfap*)dnVAMP2 expression (yellow arrows). Septate junctions distal to the paranodal astrocytes remain intact (A–C, green arrows). (D–F) A 3D reconstruction from serial block face scanning EM showing detachment of outermost paranodal loops and retraction of the outer spirals of myelin from the axon (yellow arrow) in the (*gfap*)dnVAMP2 condition. Compact myelin, magenta; axon, gray; cytoplasmic pocket of paranodal loop, tan; perinodal astrocyte, aqua. (G) Transverse section through an axon in the (*gfap*)dnVAMP2 condition where the outermost layers of myelin are filled with cytoplasm for one and one-half wraps around the axon (arrows) in withdrawing over compacted myelin. (H and I) Detachment of paranodal loops was reduced in WT and after terminating (*gfap*)dnVAMP2 expression (recovery). (J) TEM analysis of 617 adult optic nerve axons showing percentage of nodes with detached paranodal loops under various conditions [$P < 0.0001$, $\chi^2(7, n = 617) = 31.34$]. Detachment increased significantly in the (*gfap*)dnVAMP2 condition compared with -dnVAMP2 [$\chi^2(2, N = 350) = 15.882$, $P = 0.0001$]. The increase could be induced in the adult [adult onset vs. (*gfap*)dnVAMP2, $\chi^2(2, N = 246) = 0.764$, $P = 0.382$, n.s.]. Increased paranodal loop detachment was reversed after terminating expression of the transgene (recovery, 30 d) or by injecting Fondaparinux for 21 d [(*gfap*)dnVAMP2 +Fond]. The percentage of nodes with paranodal loops detached in WT mice was not significantly different from mice with (*gfap*)dnVAMP2 expression blocked (-dnVAMP2) (Movies S2 and S3). A single asterisk (*) indicates a significant difference in J and a perinodal astrocyte in H and I.

dnVAMP2 that had been treated with the thrombin inhibitor (Fig. 1 G and H). A different inhibitor, Hirudin, which inhibits thrombin by binding directly to its catalytic site, also prevented the increase in nodal gap length in (*gfap*)dnVAMP2 adult mice when delivered for 2 wk to the visual cortex via an osmotic minipump ($0.67 \pm 0.042 \mu\text{m}$ vs. $0.81 \pm 0.03 \mu\text{m}$ nodal gap length, Hirudin vs. vehicle, respectively; *t* test, $t_{16} = 2.76$, $P < 0.014$) (SI Appendix, SI Materials and Methods).

The increase in nodal gap length was reversed by supplying Dox to terminate expression of (*gfap*)dnVAMP2 from astrocytes in adult animals (recovery), but more than 5 d were required for restoration of normal gap length (Fig. 3B). Across all experimental

conditions, the length of the nodal gap was a linear function of the frequency of nodes with paranodal loops lifted (Fig. 3C), indicating that the level of paranodal loop detachment parallels the widening of the nodal gap.

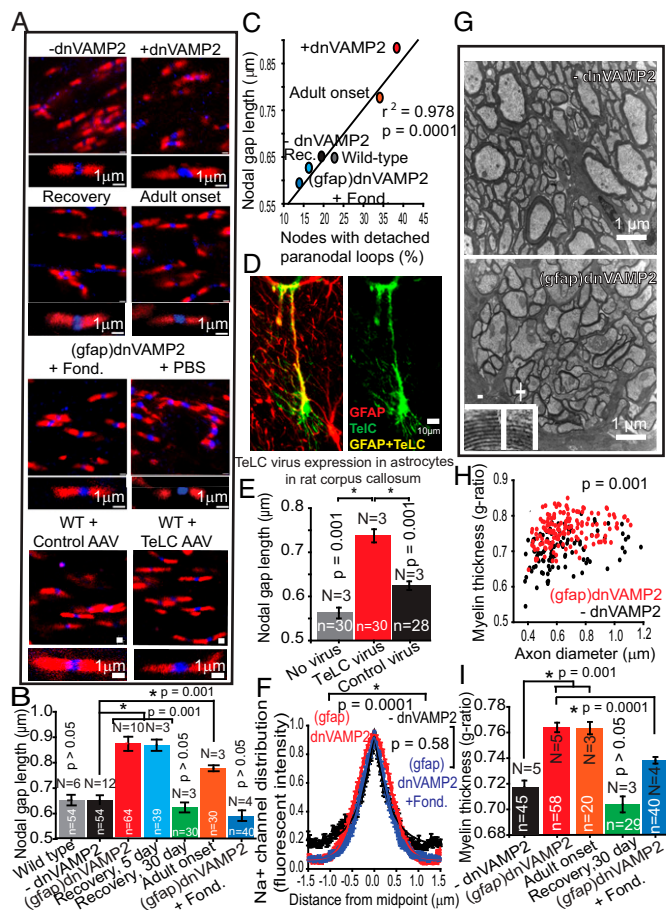


Fig. 3. Nodal morphology, nodal Na^+ channel distribution, and myelin sheath thickness regulated by vesicular release of PN1 from astrocytes. (A and B) Nodal gap length increased when astrocyte exocytosis was reduced by (*gfap*)dnVAMP2 expression throughout development or in adult mice (adult onset), but not when thrombin proteolysis was inhibited by Fondaparinux (ANOVA $F_{6, 310} = 31.83$, $P < 0.0001$). Nodal gap length recovered 30 d after terminating (*gfap*)dnVAMP2 expression, but not by 5 d. Caspr1 marking paranode, red; Na^+ channels, blue. (C) Over all experimental conditions, nodal gap length was linearly related to frequency of nodal gap detachment ($r^2 = 0.978$, $P < 0.0001$, $y = 0.0107x + 0.431$). (D) Astrocyte-specific expression of EGFP-tagged TeLC virus in corpus callosum of WT rats (green), colocalized with astrocyte marker GFAP (red). (E) Nodal gap length in regions encompassed by TeLC-transfected astrocytes was longer than in nodes outside regions of transfected astrocytes and in contralateral brain regions injected with control virus expressing EGFP (ANOVA $F_{2, 87} = 50.18$, $P < 0.0001$). (F) Na^+ channel distribution was more dispersed in nodes following (*gfap*)dnVAMP2 expression (red) and was returned to normal after treatment with Fondaparinux (blue). Half maximal width of distributions: 0.48 ± 0.0445 , 0.80 ± 0.0411 , and $0.54 \pm 0.0239 \mu\text{m}$ for black, red, and blue traces, respectively (ANOVA, $F_{2, 78} = 20.50$, $P < 0.0001$, n.s., -dnVAMP2 vs. (*gfap*)dnVAMP2, $t_{31} = 1.32$, $P = 0.58$, Bonferroni posttest). (G) Thinning of myelin when astrocyte exocytosis was reduced in adult mice [(*gfap*)dnVAMP2]. (Inset) Normal compaction of myelin sheath. (H) Thinner myelin sheath (g-ratio) in mice expressing (*gfap*)dnVAMP2 (*t* test, $t_{362} = 11.69$, $P < 0.001$). (I) Myelin sheath was thinner when astrocyte exocytosis was reduced throughout development [-dnVAMP2 vs. (*gfap*)dnVAMP2]; recovered 30 d after transgene expression was terminated and was thinned when astrocyte exocytosis was reduced in adults (adult onset). Myelin sheath thickness recovered after injection of Fondaparinux for 21 d (ANOVA, $F_{4, 190} = 33.4$, $P < 0.001$). *n* = sample size, *N* = number of animals. A single asterisk indicates a significant difference.

These findings were verified by an independent method of reducing vesicle release from astrocytes in a different brain region and in a different experimental animal (Fig. 3 *D* and *E* and *SI Appendix*, Fig. S2 *L–N*). Tetanus Toxin Light Chain (TeLC) is an adenoviral vector (AVV) that expresses TeLC specifically in astrocytes via an enhanced GFAP promoter, GfaABC₁D (*SI Appendix*, *SI Materials and Methods*), thereby inhibiting vesicular exocytosis only in transfected astrocytes (13, 14). Stereotaxic injections of TeLC and a control (benign) AVV into the corpus callosum of opposite cerebral hemispheres of WT rats resulted in specific transfection of astrocytes in the vicinity of the injection (Fig. 3*D* and *SI Appendix*, Fig. S2*L*), identified by the EGFP reporter. Confocal images of nodes of Ranvier in microscope fields covered by a transfected astrocyte were obtained, and the length of the nodal gap was measured. Twenty-one days post injection, the mean nodal gap length of axons encompassed by TeLC-infected astrocytes was significantly larger than that in the control AVV-infected astrocytes in the contralateral corpus callosum (TeLC vs. control virus, Fig. 3*E*). Since astrocytes form nonoverlapping domains (15), an analysis was also made of nodes of Ranvier in microscope fields within the domain of transfected astrocytes expressing EGFP (*SI Appendix*, Fig. S2 *L* and *N*) and in microscopic fields in the same region but outside the domain of a transfected astrocyte, where astrocytes lacked GFP expression (*SI Appendix*, Fig. S2 *L* and *M*). Nodal gap length in axons encompassed by TeLC-transfected astrocytes was significantly larger than nodal gap length of axons encompassed by untransfected astrocytes in the same microscopic field (Fig. 3*E*). Together, these results indicate that astrocytic exocytosis regulates nodal gap length via inhibition of thrombin-mediated proteolysis of NF155. Moreover, these effects are regulated within the spatial domain of individual astrocytes rather than being a systemic effect.

Distribution of Na⁺ Channels at the Node of Ranvier. Nodal gap length and Na⁺ channel distribution in the node of Ranvier have a strong influence on action potential firing and CV (4). Detachment of outer wraps of myelin from the axon and widening of the nodal gap could allow lateral diffusion of Na⁺ channels at the node of Ranvier. Sodium channel distribution in the nodal gap was measured by line-scan densitometry across the node using high-magnification confocal microscopy and was found to be broader when exocytosis from astrocytes was reduced by (*gfap*)dnVAMP2 expression (Fig. 3*F*). Treating animals expressing (*gfap*)dnVAMP2 with the thrombin inhibitor prevented the dispersion of Na⁺ channels (Fig. 3*F*), indicating a mechanism dependent on thrombin proteolysis, consistent with the lifting of paranodal loops increasing nodal gap length.

Thus, the distribution of Na⁺ channels inside the node of Ranvier becomes broader as the nodal gap widens when exocytosis in astrocytes is reduced. Both the decreased transmembrane current density resulting from redistribution of Na⁺ channels, even without changes in their abundance, and the increased membrane capacitance from lengthening the nodal gap would slow activation of action potentials at the node. Together, these results indicate a reversible process regulating Na⁺ channel distribution at the node by exocytosis from astrocytes acting through inhibition of thrombin-dependent proteolysis.

Astrocyte Exocytosis Regulates Thickness of the Myelin Sheath. Nodal remodeling could be associated with changes in thickness of the myelin sheath because the paranodal loop that borders the nodal gap is formed from the outermost layer of myelin, which is continuous with the plasma membrane of the oligodendrocyte through a slender process (the outer mesaxon or outer cytoplasmic tongue) (16). Quantitative TEM analysis showed that myelin sheath thickness was reduced significantly when exocytosis in astrocytes was reduced (Fig. 3 *G–J*). The interlamellar distance within the compact myelin sheath did not differ, indicating normal compaction of myelin (Fig. 3*G*, *Inset*). Myelin thickness

recovered to normal after terminating the VAMP2-dependent reduction in exocytosis in astrocytes by administering Dox to the feed at postnatal day 40 (P40) and examining myelin thickness at P70 (Fig. 3*J*). Thinning of the myelin sheath was also induced when exocytosis from astrocytes was decreased in adults after formation of compact myelin (Fig. 3*I*). Treatment with the thrombin inhibitor Fondaparinux reversed the effects (Fig. 3*J*), and there was no change in axon diameter or number of unmyelinated axons with dnVAMP2 expression (*SI Appendix*, Fig. S3 *Q* and *R*).

Regulation of Conduction Velocity in the Optic Nerve as a Consequence of Remodeling of Nodal Gap and Myelin Thickness. Mathematical modeling based on passive cable properties predicted a CV decrease of ~11% from the observed changes in myelin structure after reducing exocytosis from astrocytes (17, 18). Consistent with this prediction, electrophysiological recordings in excised optic nerve showed that CV was reduced $20.4 \pm 1.8\%$ in the mice expressing (*gfap*)dnVAMP2 (Fig. 4 *A–E* and *SI Appendix*, Fig. S6). The mathematical model does not take into consideration the reduced clustering of Na⁺ channels, which could have led to an underestimate of the predicted reduction in CV when exocytosis in astrocytes was reduced.

Regulation of Latency of Spike-Time Arrival in the Visual Cortex as a Consequence of Remodeling Nodal Gap and Myelin Thickness. High temporal precision of conduction time between synaptic relay points in the CNS is critical for optimal performance of neural circuits (19), and pathological conditions that desynchronize spike-time arrival can cause neurological and psychological dysfunction (20). We therefore measured visually evoked electrophysiological responses in the visual cortex (Fig. 4 *F–I*) and measured visual acuity by the optomotor reflex (Fig. 4 *J–L*). Latency to the peak visually evoked potentials (VEP) in the visual cortex was significantly longer in mice expressing (*gfap*)dnVAMP2 in astrocytes (Fig. 4 *F–H*), consistent with the reduced CV measured in excised optic nerve axons. Visual acuity was also significantly decreased in mice expressing (*gfap*)dnVAMP2 in astrocytes (Fig. 4*K*). Daily injection of Fondaparinux for 21 d restored the

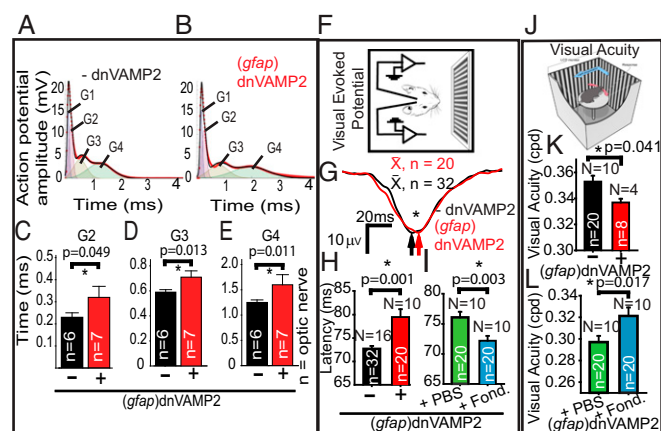


Fig. 4. Myelin plasticity changes conduction velocity, spike-time arrival in visual cortex, and visual acuity. (*A–E*) Conduction times were slower for all components of the compound action potential [G2 (*t* test, $t_{11} = 2.21$), G3 (*t* test, $t_{11} = 3.05$), and G4 (*t* test, $t_{11} = 3.05$)] that could be measured in excised optic nerves in the (*gfap*)dnVAMP2, compared with the -dnVAMP2 condition. (*F*) VEPs in visual cortex. (*G–I*) Latency to peak VEP was 6.74 ms longer in the (*gfap*)dnVAMP2 condition (*G* and *H*, *t* test, $t_{50} = 4.52$) and restored by Fondaparinux treatment (*I*, *t* test, $t_{38} = 3.17$). *G* shows summed waveforms for all data in *H*. (*J–L*) Visual acuity measured by computerized striped-drum assay was reduced in the (*gfap*)dnVAMP2 condition (*K*, *t* test, $t_{50} = 2.23$), and the effect was reversed by Fondaparinux (*L*, *t* test, $t_{38} = 2.49$). A single asterisk (*) indicates a significant difference.

latency to peak VEP (Fig. 4I) and the deficit in visual acuity (Fig. 4L) in mice expressing (*gfap*)dnVAMP2, indicating a thrombin-dependent mechanism.

In longitudinal studies on the same individual mice in the VEP studies, we found that restoring normal levels of exocytosis in astrocytes for 5 d did not change nodal gap length (Fig. 3B) or latency to VEP (SI Appendix, Fig. S7A), even though expression of (*gfap*)dnVAMP2 was completely inhibited at this time point (SI Appendix, Fig. S2J). Thirty days were required for recovery of nodal gap length (Fig. 3B) and for recovery of NF155 cleavage (SI Appendix, Fig. S7B). These kinetics are consistent with the proposed mechanism for the structural and functional changes in myelin via vesicular release of protease inhibitors from astrocytes regulating thrombin-dependent cleavage of NF155.

Discussion

The functions of perinodal astrocytes are not well understood, and before this research there was no theory for how the myelin sheath could be thinned nondestructively. Together, the results show that exocytosis of thrombin protease inhibitors from astrocytes inhibits cleavage of NF155 at a thrombin protease site in the extracellular domain, regulating detachment of the outermost paranodal loops of myelin from the axon. The astrocyte-mediated effects on myelin structure have electrophysiological and functional consequences; they are reversible, and they can proceed in compacted myelin of adults. This process occurs normally in WT animals, but it is greatly increased when exocytosis from astrocytes is reduced. Moreover, viral transfection of individual astrocytes shows that myelin morphology, and thus impulse conduction, are regulated locally within the spatial domain encompassed by individual astrocytes.

Genetic loss of NF155 and other components of the paranodal septate junctions further support the present findings. Loss of the septate junctions by various genetic causes results in detachment of the paranodal loops, widening of the nodal gap, dispersion of ion channels at the node, and reduced CV (21–23). In contrast to proteolytic cleavage of only the outermost paranodal loops from the axon by reducing exocytosis in astrocytes, genetic disruption of all of the junctions results in dysmyelination and failure to maintain compact myelin (myelin splitting, decompaction—and thus thicker sheaths—vacuolation, and loss of myelin) (24).

Thrombin would seem well suited for myelin remodeling because its activity is tightly constrained by a complex network of positive and negative factors that are highly regulated spatially and temporally, as is evident in thrombin proteolysis in the blood coagulation cascade (25). Astrocytes are a primary source of PN1 and other protease inhibitors, but they are also the major cellular source of the enzyme Tissue Factor, which initiates the conversion of prothrombin to thrombin (26). Thus, perinodal astrocytes are equipped to locally promote or inhibit thrombin activity at the paranodal loops flanking astrocytes at the nodes of Ranvier. Astrocyte secretome shows no evidence for thrombin expression under normal conditions (27), but astrocytes can express thrombin under certain pathological conditions, such as Alzheimer's disease (28).

Exocytosis of other molecules from astrocytes is likely reduced by the dnVAMP2 and TeLC transgenes (29), but a thrombin-dependent mechanism for these anatomical, physiological, and functional changes is shown by reversing all of these effects by the highly specific thrombin inhibitor Fondaparinux. Hirudin, a thrombin inhibitor operating through a different mechanism, also prevents the increase in nodal gap length when exocytosis from astrocytes is reduced. These data exclude exocytosis of neurotransmitters (ATP and glutamate) from astrocytes as being responsible, but they do not rule out possible involvement of additional signaling molecules from astrocytes, other cell adhesion molecules, or other functions of thrombin in myelin remodeling.

The results suggest that the myelin sheath can be thickened and thinned by different cellular processes of membrane addition and

retrieval in oligodendrocytes. The myelin sheath is formed by the inner glial tongue (an extension from the oligodendrocyte cell body), which is in contact with the axon. The inner tongue spirals around the axon to form multiple layers of compact myelin and expands laterally (30). As the axon grows and increases in caliber, more layers of myelin are added by the inner tongue, and the internodal distance increases. This growth requires movement between the layers of myelin, and it is well appreciated that the myelin sheath is a dynamic membrane system in which the layers can slip over each other to thicken the sheath (16). The outermost paranodal loop of myelin is continuous with the plasma membrane of the oligodendrocyte through the outer mesaxon, so that detachment of the outer paranodal loop and retraction into the oligodendrocyte thins the myelin sheath and widens the nodal gap. These changes and dispersed Na⁺ channels slow CV.

A decrease in visual acuity accompanied the increased VEP latency in parallel with myelin thinning and nodal gap widening caused by the thrombin-dependent cleavage of NF155 when exocytosis was reduced in astrocytes. This visual impairment is consistent with studies showing that conduction delays can degrade sensory perception and that compensatory mechanisms are necessary to optimize spike-time arrival. As optic nerve length increases with growth in teleost fish, the diameter of retinal axons increases to preserve the timing of visual information arriving at the brain (31). Myelin thickness also increases to maintain the optimal g-ratio (32). Loss of visual acuity is an early diagnostic indication of multiple sclerosis (MS) (33), and VEP amplitudes are reduced in MS patients even before visual impairment (34). The present findings add a mechanism to adjust conduction delays in individual axons to promote optimal spike-time arrival and behavioral performance.

In addition to precise spike-time arrival, neural oscillations of proper frequency and phase are critical for information processing by coordinating activity among groups of neurons. Despite the several-thousand-fold increase in volume of the mammalian brain across species, the hierarchy of brain oscillations remains preserved to enable multiple timescale communication within and across neuronal networks at approximately the same speed, irrespective of brain volume (35). Conduction delays between distant brain regions will profoundly affect the phase and amplitude coupling, and thus the stability of neural oscillations (36). For example, fast field oscillations in the CA1 region of the hippocampus participate in transferring hippocampal information to the basolateral amygdala (37) and cortex (38) for consolidation of context-dependent memory. While local circuit properties, which can be modulated by astrocytes (39), govern neural oscillations locally, myelination of axons projecting between distant brain regions must be appropriate to maintain, or possibly change, conduction delays to sustain phase coupling of neural oscillations.

Many processes are involved in establishing appropriate myelination on individual axons, but perinodal astrocytes provide a mechanism of remodeling that could help establish and maintain proper myelin thickness and nodal properties necessary for the optimal conduction latencies in neural circuits. By regulating myelin structure and CV, perinodal astrocytes could also contribute to structural modifications of white matter seen in animal studies and by human brain magnetic resonance imaging after various learning tasks (20). Further research will be required to determine if astrocyte remodeling of myelin structure is modified by neural impulse activity. Chemically induced exocytosis of PN1 in cultured astrocytes does not predict physiologically induced exocytosis, but the Ca²⁺ dependency of exocytosis supports the possibility of modulating these perinodal astrocyte functions by ligand or ion-gated calcium channels activated by neuronal firing.

Many studies have used this transgenic mouse to study the effects of exocytosis from astrocytes, and the model is well characterized (12, 29), but none have concerned myelin. With the exception of certain neurogenic regions, where GFAP can be

expressed transiently in neural progenitor cells, these studies show that the gene is expressed only in astrocytes under strict Dox control, as was the case in our studies. One study, however, reported expression of the gene in some neurons (40), prompting us to use an independent method to reduce vesicle release from astrocytes by using viral transfection of tetanus toxin in WT rats, and the results matched the findings using the dnVAMP2 transgenic mouse. No effects on retinal activity were evident in this transgenic mouse by electroretinogram analysis, and none would be expected because GFAP is not expressed in Müller glia under normal conditions, and blocking exocytosis from Müller glia using botulinum neurotoxin B has no effects on retinal responses (41).

The actions of astrocytes in regulating myelin and nodal structure could be relevant to myelin disorders. Abnormalities in astrocytes can lead to leukodystrophies, such as in Alexander's disease and neuromyelitis optica (42). Conditions increasing CNS thrombin levels, such as hypoxia or injury, or impairing exocytosis in astrocytes could promote cleavage of NF155 and detachment of myelin from the axon. Expression of NF155 is altered near active demyelinating lesions in multiple sclerosis (43), and paranodal septate junctions are compromised with age, followed by myelin disruption (44). The mechanism for these age-related changes is unknown, but thrombin can be produced locally in brain tissue in association with neurofibrillary tangles in Alzheimer's disease and

Parkinsonism dementia (45), and astrocytes begin to express thrombin in Alzheimer's disease (28). Therapies to promote recovery from demyelinating disease may be possible by targeting perinodal astrocytes and thrombin-mediated cleavage of NF155.

Materials and Methods

For full details, see *SI Appendix, SI Materials and Methods*.

Exocytosis in astrocytes was reduced by two methods: an astrocyte-specific viral vector to express tetanus toxin light chain in astrocytes in the corpus callosum of rats and a transgenic mouse expressing a fragment of VAMP2 in astrocytes studied in the optic nerve and visual cortex. All research involving animals was approved by the Institutional Animal Care and Use Committee, Eunice Kennedy Shriver National Institute of Child Health and Human Development, National Institutes of Health.

ACKNOWLEDGMENTS. We thank K. McCarthy and K. Casper for providing transgenic mice; S. Kasparov for the TeLC viral vector; H. Qian and Y. Li (National Eye Institute Visual Function Core); L. Dye and L. Holtzclaw [National Institute of Child Health and Human Development (NICHD)] Imaging Core; D. Abebe, for maintaining animal health; E. Benson and G. Kidd (Renovo, Inc.) for assistance with SBSEM and 3D reconstruction; Y. Li, for LC-mass spectrometry; N. Sinaï, for statistical advice; M. Robnett for part of Fig. 3I; and A. Koretsky (National Institute of Neurological Disorders and Stroke) for donating laboratory space. Research was supported by an intramural program of NICHD (Grant ZIAHD000713-22), Center for Information Technology, National Cancer Institute, and the Department of Defense (Grant 11162432) through the Henry M. Jackson Foundation for the Advancement of Military Medicine.

- Fields RD (2015) A new mechanism of nervous system plasticity: Activity-dependent myelination. *Nat Rev Neurosci* 16:756–767.
- Serwanski DR, Jukkola P, Nishiyama A (2017) Heterogeneity of astrocyte and NG2 cell insertion at the node of Ranvier. *J Comp Neurol* 525:535–552.
- Black JA, Waxman SG (1988) The perinodal astrocyte. *Glia* 1:169–183.
- Rios JC, et al. (2003) Paranodal interactions regulate expression of sodium channel subtypes and provide a diffusion barrier for the node of Ranvier. *J Neurosci* 23:7001–7011.
- Waxman SG, Pappas GD, Bennett MV (1972) Morphological correlates of functional differentiation of nodes of Ranvier along single fibers in the neurogenic electric organ of the knife fish *Stern archus*. *J Cell Biol* 53:210–224.
- Charles P, et al. (2002) Neurofascin is a glial receptor for the paranodin/Caspr/contactin axonal complex at the axoglial junction. *Curr Biol* 12:217–220.
- Binnie CG, Lord ST (1993) The fibrinogen sequences that interact with thrombin. *Blood* 81:3186–3192.
- Thaxton C, et al. (2010) *In vivo* deletion of immunoglobulin domains 5 and 6 in neurofascin (Nfasc) reveals domain-specific requirements in myelinated axons. *J Neurosci* 30:4868–4876.
- Dihanich M, Kaser M, Reinhard E, Cunningham D, Monard D (1991) Prothrombin mRNA is expressed by cells of the nervous system. *Neuron* 6:575–581.
- Choi BH, Suzuki M, Kim T, Wagner S, Cunningham DD (1990) Protease nexin-1. Localization in the human brain suggests a protective role against extravasated serine proteases. *Am J Pathol* 137:741–747.
- Giau R, Carrette J, Bockaert J, Homburger V (2005) Constitutive secretion of protease nexin-1 by glial cells and its regulation by G-protein-coupled receptors. *J Neurosci* 25:8995–9004.
- Pascual O, et al. (2005) Astrocytic purinergic signaling coordinates synaptic networks. *Science* 310:113–116.
- Sheikhabaie S, et al. (2018) Astrocytes modulate brainstem respiratory rhythm-generating circuits and determine exercise capacity. *Nat Commun* 9:370.
- Angelova PR, et al. (2015) Functional oxygen sensitivity of astrocytes. *J Neurosci* 35:10460–10473.
- Bushong EA, Martone ME, Jones YZ, Ellisman MH (2002) Protoplasmic astrocytes in CA1 stratum radiatum occupy separate anatomical domains. *J Neurosci* 22:183–192.
- Morell P, Quarles RH (1999) The myelin sheath. *Basic Neurochemistry: Molecular, Cellular and Medical Aspects*, eds. Siegel GJ, Agranoff BW, Albers RW, Fisher SK, Uhler MD (Lippincott-Raven, Philadelphia), 6th Ed.
- Basser PJ (1993) Cable equation for a myelinated axon derived from its microstructure. *Med Biol Eng Comput* 31(Suppl 1):S87–S92.
- Basser PJ (2004) Scaling laws for myelinated axons derived from an electrotonic core-conductor model. *J Integr Neurosci* 3:227–244.
- Dan Y, Poo MM (2006) Spike timing-dependent plasticity: From synapse to perception. *Physiol Rev* 86:1033–1048.
- Fields RD (2008) White matter in learning, cognition and psychiatric disorders. *Trends Neurosci* 31:361–370.
- Pillai AM, et al. (2009) Spatiotemporal ablation of myelinating glia-specific neurofascin (Nfasc^{NF155}) in mice reveals gradual loss of paranodal axoglial junctions and concomitant disorganization of axonal domains. *J Neurosci Res* 87:1773–1793.
- Bhat MA, et al. (2001) Axon-glia interactions and the domain organization of myelinated axons requires neuexin IV/Caspr/paranodin. *Neuron* 30:369–383.
- Çolakoglu G, Bergstrom-Tyrberg U, Berglund EO, Ranscht B (2014) Contactin-1 regulates myelination and nodal/paranodal domain organization in the central nervous system. *Proc Natl Acad Sci USA* 111:E394–E403.
- Rosenbluth J, Mierzwa A, Shroff S (2013) Molecular architecture of myelinated nerve fibers: Leaky paranodal junctions and paranodal dysmyelination. *Neuroscientist* 19:629–641.
- Wang Y, Luo W, Reiser G (2008) Trypsin and trypsin-like proteases in the brain: Proteolysis and cellular functions. *Cell Mol Life Sci* 65:237–252.
- Eddleston M, et al. (1993) Astrocytes are the primary source of tissue factor in the murine central nervous system. A role for astrocytes in cerebral hemostasis. *J Clin Invest* 92:349–358.
- Dowell JA, Johnson JA, Li L (2009) Identification of astrocyte secreted proteins with a combination of shotgun proteomics and bioinformatics. *J Proteome Res* 8:4135–4143.
- Arai T, Miklossy J, Klegeris A, Guo J-PP, McGeer PL (2006) Thrombin and prothrombin are expressed by neurons and glial cells and accumulate in neurofibrillary tangles in Alzheimer disease brain. *J Neuropathol Exp Neurol* 65:19–25.
- Guček A, et al. (2016) Dominant negative SNARE peptides stabilize the fusion pore in a narrow, release-unproductive state. *Cell Mol Life Sci* 73:3719–3731.
- Snaidero N, et al. (2014) Myelin membrane wrapping of CNS axons by PI(3,4,5)P₃-dependent polarized growth at the inner tongue. *Cell* 156:277–290.
- Bakken TE, Stevens CF (2012) Visual system scaling in teleost fish. *J Comp Neurol* 520:142–153.
- Waxman SG (1980) Determinants of conduction velocity in myelinated nerve fibers. *Muscle Nerve* 3:141–150.
- Regan D, Silver R, Murray TJ (1977) Visual acuity and contrast sensitivity in multiple sclerosis—Hidden visual loss: An auxiliary diagnostic test. *Brain* 100:563–579.
- Diem R, Tschirne A, Bähr M (2003) Decreased amplitudes in multiple sclerosis patients with normal visual acuity: A VEP study. *J Clin Neurosci* 10:67–70.
- Buzsáki G, Logothetis N, Singer W (2013) Scaling brain size, keeping timing: Evolutionary preservation of brain rhythms. *Neuron* 80:751–764.
- Pajević S, Basser PJ, Fields RD (2014) Role of myelin plasticity in oscillations and synchrony of neuronal activity. *Neuroscience* 276:135–147.
- Girardeau G, Inema I, Buzsáki G (2017) Reactivations of emotional memory in the hippocampus-amygdala system during sleep. *Nat Neurosci* 20:1634–1642.
- Khodagholy D, Gelinas JN, Buzsáki G (2017) Learning-enhanced coupling between ripple oscillations in association cortices and hippocampus. *Science* 358:369–372.
- Lee HS, et al. (2014) Astrocytes contribute to gamma oscillations and recognition memory. *Proc Natl Acad Sci USA* 111:E3343–E3352.
- Fujita T, et al. (2014) Neuronal transgene expression in dominant-negative SNARE mice. *J Neurosci* 34:16594–16604.
- Slezak M, et al. (2012) Relevance of exocytotic glutamate release from retinal glia. *Neuron* 74:504–516.
- Lanciotti A, et al. (2013) Astrocytes: Emerging stars in leukodystrophy pathogenesis. *Transl Neurosci*, 4.
- Howell OW, et al. (2006) Disruption of neurofascin localization reveals early changes preceding demyelination and remyelination in multiple sclerosis. *Brain* 129:3173–3185.
- Shepherd MN, Pomier AD, Velazco CS, Henderson SC, Dupree JL (2012) Paranodal reorganization results in the depletion of transverse bands in the aged central nervous system. *Neurobiol Aging* 33:203.e13–203.e24.
- Krenzlin H, Lorenz V, Danckwardt S, Kempki O, Alessandri B (2016) The importance of thrombin in cerebral injury and disease. *Int J Mol Sci* 17:84.